

Atomic Control of Conductivity Versus Ferromagnetism in Wide-Gap Oxides Via Selective Doping: V, Nb, Ta in Anatase TiO₂

Jorge Osorio-Guillén, Stephan Lany, and Alex Zunger

National Renewable Energy Laboratory, Golden, Colorado 80401, USA

(Received 26 January 2007; published 23 January 2008)

We identify two general types of electronic behaviors for transition-metal impurities that introduce excess electrons in oxides. (i) The dopants introduce resonant states inside the host conduction band and produce free electrons; (ii) the dopants introduce a deep gap state that carries a magnetic moment. By combining electronic structure calculations, thermodynamic simulations, and percolation theory, we quantify these behaviors for the case of column V-B dopants in anatase TiO₂. Showing behavior (i), Nb and Ta dopants can convert the insulator TiO₂ into a transparent conductor. Showing behavior (ii), V dopants could convert nonmagnetic TiO₂ into a ferromagnet. Whether a dopant shows behavior (i) or (ii) is encoded in its atomic *d* orbital energy.

DOI: 10.1103/PhysRevLett.100.036601

PACS numbers: 72.20.Jv, 71.20.Mq, 75.50.Pp, 77.84.Bw

TiO₂ has become an important wide-band gap oxide because of its ability to be a good solvent for numerous impurities [1,2]. Indeed, transition-metal doping of anatase TiO₂ is proposed to lead to a ferromagnetic wide-gap oxide [3,4], or to transparent conductivity [5–7], making anatase a promising candidate for an unconventional transparent conducting oxide (TCO) based on transition metals. Here we address theoretically the design principles for transparent conductivity and for ferromagnetism in oxides. We suggest a simple criterion that the position of the atomic *d* orbital energies of the early transition-metal dopants is the indicator determining whether the dopant is an electron producer, leading to conductive but nonmagnetic behavior, or whether the dopant is magnetic, leading to ferromagnetic but nonconductive behavior.

To design a “transparent conductor” one needs to identify impurities that are (i) soluble in the host, (ii) able to shed their outer electrons, transferring them to the host conduction band minimum (CBM). Furthermore, most importantly (iii) the host material must not form “antibodies” in the form of intrinsic structural defects created in response to such external doping by electrons and compensate the latter [8]. For example, most wide-gap oxides will spontaneously form cation vacancies in response to deliberate introduction of free electrons [9]. We show that, remarkably, anatase TiO₂ has a rather high formation energy for cation vacancies (under metal-rich growth conditions) and will thus tolerate introduction of free electrons without compensating them. Experimentally one observes that TiO₂ shows electron densities of only up to 10¹⁸ cm⁻³, generally associated with a partial loss in transparency (blue coloration) [10]. This has been attributed to unintentional doping by hydrogen [11,12]. To exceed this level of free electron concentration (10¹⁸ cm⁻³), we consider here extrinsic electron doping by substituting the group IV-B host element Ti with a group V-B transition-metal impurity V, Nb, and Ta. Exhibiting high 4*d* and 5*d* atomic orbital energies (see Fig. 1), Nb and Ta are more likely [13] to

transfer their excess electron to the host CBM than V having a much lower 3*d* atomic orbital energy [14]. We have examined quantitatively such design principles [8] via first-principles calculations and thermodynamic modeling, finding that the room-temperature free electron density of pure (H-free) TiO₂ is negligible ($n \leq 10^{14}$ cm⁻³) but can be raised into the 10²¹ cm⁻³ range via either Nb or Ta doping.

To design a “ferromagnetic semiconductor,” one needs to identify a dopant which (i) carries a magnetic moment in its stable charge state [9,15], which (ii) exhibits ferromagnetic coupling between such impurities within a certain range of magnetic interaction, and which (iii) has a thermodynamic solubility above the magnetic percolation threshold given this range of interaction [9,16]. We have previously found that the existence of partially-occupied impurity orbital within the band gap of the host material would facilitate the stability of ferromagnetic interactions among such impurities [15]. We find for V dopants in TiO₂ that (i) V_{Ti}⁰ create a partially occupied gap state with open-shell *d*-based electronic configuration $t_{2+}^1 t_{2-}^1 e_+^0 e_-^0$ (referring to the approximate local O_h site symmetry) and magnetic moment of 1μ_B/V, due to the lower 3*d* energy of V

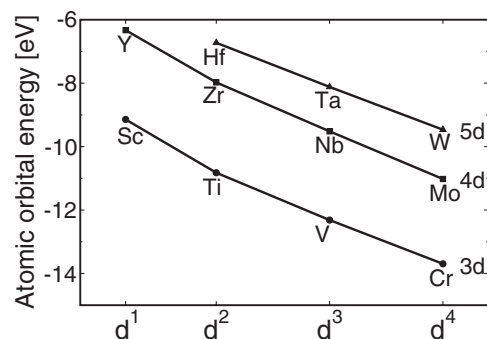


FIG. 1. Calculated Dirac-Fock atomic *d*-orbital energies for neutral atoms [14].

compared to the respective $4d$ and $5d$ energies of Nb and Ta, (ii) V_{Ti} - V_{Ti} pairs couple ferromagnetically, and the range of interaction extends up to the fifth neighbor, and (iii) the equilibrium solubility of V reaches a maximum of $x = 21\%$ (cation substitution), being above the percolation threshold $x_p = 5.6\%$ calculated for fifth-nearest-neighbor interaction in the anatase lattice [17]. Thus, V doping of TiO_2 could lead to ferromagnetism under appropriate growth conditions that provide sufficiently high V concentrations.

This work shows how design principles, distilled from previous theoretical calculations [8,9,15,16], can offer reasonable guesses for establishing specific electronic behavior in oxides, including transparent conductivity and ferromagnetism, using elements from the same column in the periodic table. Based on the present results for column V-B dopants in anatase TiO_2 , we suggest that electron doping with $4d$ and $5d$ elements (e.g., Zr and Hf in In_2O_3 , Nb and Ta in SnO_2) can generally be used to design TCOs, whereas $3d$ doping tends to produce nonconducting, magnetic states (e.g., Ti in In_2O_3 , V in SnO_2).

Method.—All total energies, atomic forces, and magnetic moments were calculated via first principles using the projector augmented wave method and the generalized gradient approximation (GGA-PBE) as implemented in the VASP code [18]. We calculate the formation enthalpy [19] $\Delta H_{D,q}(E_F, \mu)$ of defect D in charge state q (Fig. 2 shows ΔH for $D = Ti$ or O vacancies, Ti interstitial, and V, Nb, or Ta impurities) as a function of the Fermi energy E_F and the chemical potential μ of Ti, V, Nb, Ta, and O using

the supercell method by

$$\Delta H_{D,q}(E_F, \mu) = [E_{D,q} - E_H] + \sum n_\alpha \mu_\alpha + q(E_v + \Delta E_F). \quad (1)$$

Here, $E_{D,q}$ is the total energy of the supercell containing the defect D in charge state q , and E_H is the energy of the pure host supercell. The calculated supercell total energies are corrected for deficiencies associated with the supercell formalism and with the GGA approximation according to Refs. [13,19]. The second term in Eq. (1) describes the chemical reservoir in equilibrium, where $n_\alpha = \mp 1$ if an atom is added ($-$) or removed ($+$) in order to form the defect. The chemical potential $\mu_\alpha = \mu_\alpha^{elem} + \Delta\mu_\alpha$ of the added (removed) ion α is given with respect to the chemical potential of the elemental phase, μ_α^{elem} , for which we choose the solid phase except for oxygen, where we use the O_2 molecule. The third term in Eq. (1) is the energy of the electron reservoir, i.e., the Fermi energy $E_F = E_v + \Delta E_F$, which can range from the valence band maximum—VBM—(E_v) to the CBM (E_c). Here we take $E_c(T)$ as a function of temperature to account for the temperature dependence of the band gap [20]. The electrical transition levels $\epsilon(q/q')$ (dots in Fig. 2) between two charge states q and q' within the band gap are calculated as the Fermi energy at which $\Delta H_{D,q} = \Delta H_{D,q'}$. Figure 3 illustrates the range of possible growth conditions between the Ti-rich–O-poor limit [$\Delta\mu_{Ti} = -1.5$ eV, $\Delta\mu_O = -3.84$ eV (Ti_2O_3 boundary, “ α ” in Fig. 3)] and the extreme O-rich–Ti-poor limit [$\Delta\mu_{Ti} = \Delta H_f(TiO_2) = -9.18$ eV,

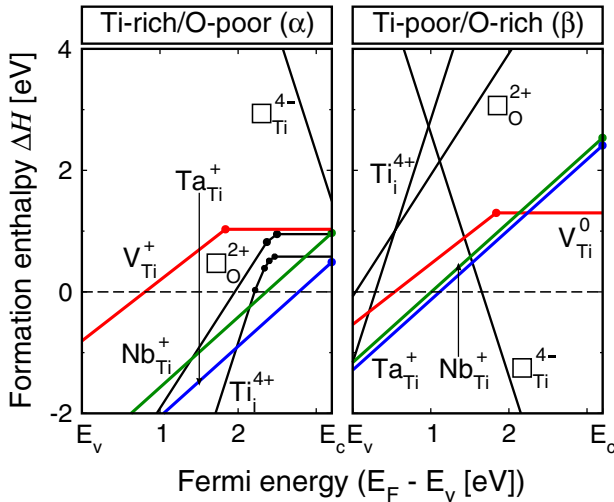


FIG. 2 (color online). Calculated formation enthalpies for anion vacancy (\square_O) and cation vacancy (\square_{Ti}), Ti_i , V_{Ti} , Nb_{Ti} , and Ta_{Ti} in anatase TiO_2 as a function of the Fermi energy. The dots mark transition levels between different charge states. Ti-rich–O-poor conditions refer to line “ α ” in Fig. 3, and O-rich–Ti-poor conditions refer to line “ β ,” i.e., the extreme O-rich condition ($\Delta\mu_O = 0$). Note that, generally, $\Delta\mu_O(P, T) \ll 0$ under realistic conditions (e.g., “ γ ” in Fig. 3).

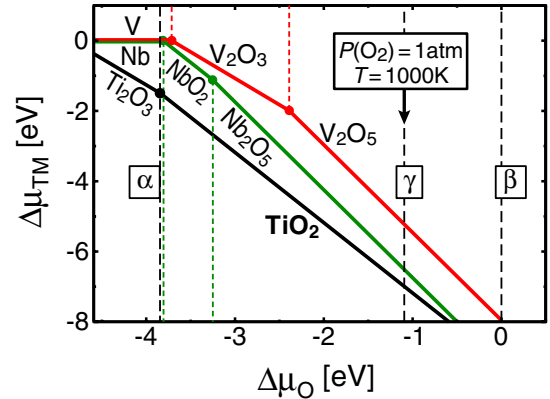


FIG. 3 (color online). The transition-metal chemical potentials $\Delta\mu_{TM}$ (TM = Ti, V, Nb) as a function of the O chemical potential $\Delta\mu_O$, as derived from the host stability conditions $x\Delta\mu_{TM} + y\Delta\mu_O = \Delta H_f(TM_xO_y)$ of different oxide stoichiometries. The vertical lines separate the ranges of $\Delta\mu_O$ where $\Delta\mu_{TM}$ is determined by the formation of one given stoichiometry (including the metallic phases of Nb and V). The lines α , β , and γ indicate, respectively, for the growth of anatase TiO_2 , the Ti-rich condition (Ti_2O_3 boundary, $\Delta\mu_O = -3.84$ eV), the extreme O-rich condition [$\Delta\mu_O = 0$], and a realistic O-rich condition [$p(O_2) = 1$ atm, $T = 1000$ K, $\Delta\mu_O = -1.09$ eV].

$\Delta\mu_{\text{O}} = 0$ eV, “ β ” in Fig. 3]. In order to simulate realistic growth conditions, we calculate the oxygen chemical potential $\Delta\mu_{\text{O}}$ for the O_2 gas phase at finite temperature T and pressure P [9] (see “ γ ” in Fig. 3”). The thermodynamic simulations for the oxide stoichiometry and the carrier densities follow our previous work on ZnO and In_2O_3 [13,21].

Intrinsic defects.—Figures 4(a) and 4(b) show the local density of states introduced by neutral oxygen vacancy \square_{O}^0 and titanium interstitial Ti_i^0 in TiO_2 , respectively. We see that these defects introduce deep states in the (GGA-corrected) gap, and hence, are not easily ionized. Thus, our interpretation differs from that in Ref. [22], where it was suggested that these defects do not introduce levels in the (uncorrected) local density approximation (LDA) band gap. Our finding of deep levels for \square_{O} and Ti_i is, however, corroborated by theoretical results applying Coulomb energy corrections like the LDA + U method [23,24]. Figure 2 shows the calculated defect formation and transition energies in TiO_2 . We see that indeed both \square_{O} and Ti_i have their donor transition levels $\epsilon(0/+)$ rather deep at $E_c - 0.7$ eV. Considering equilibrium growth of anatase TiO_2 at, e.g., $T_{\text{growth}} = 1000$ K, we find considerable concentrations of \square_{O} and Ti_i up to the 10^{19} cm^{-3} range under Ti-rich–O-poor conditions (Fig. 5) resulting from low formation enthalpies ΔH of \square_{O} and Ti_i below 1 eV under Ti-rich–O-poor growth conditions. Because of the deep transition levels of \square_{O} and Ti_i , however, the room-temperature electron density stays below $\leq 10^{14}$ cm^{-3} in pure TiO_2 . Indeed, the higher electron densities of 10^{18} cm^{-3} , found experimentally in nominally undoped anatase samples exhibiting a bluish color [10], was later attributed to hydrogen [11], being present as an unintentional dopant [12]. Consistent with our finding of low electron densities in pure TiO_2 , a strong increase in resistivity and the restoration of transparency were observed in Ref. [10] upon

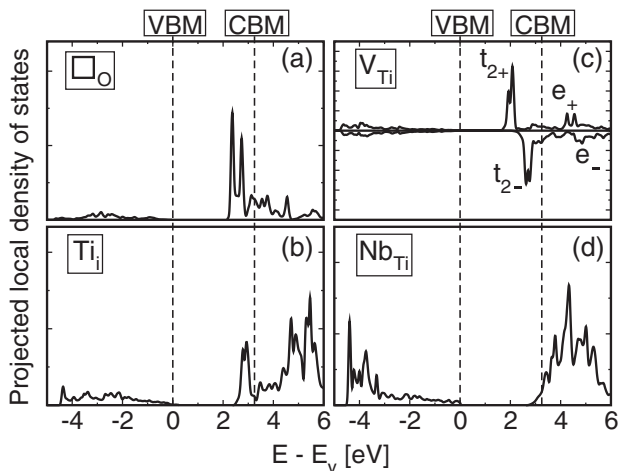


FIG. 4. Calculated local density of states (DOS) for \square_{O}^0 , Ti_i^0 , V_{Ti}^0 , and Nb_{Ti}^0 using GGA. The hosts VBM and CBM are indicated by vertical-dashed lines.

annealing in ambient atmosphere, which probably removed hydrogen.

We recently predicted that oxygen vacancy in In_2O_3 and ZnO , despite having a deep $\epsilon(0/2+)$ donor level can cause conductivity through a metastable shallow vacancy state [13,21]. The existence of such a shallow state requires that the deep gap level of the neutral \square_{O} becomes resonant inside the conduction band after photoionization. We do not find such behavior in the more ionic TiO_2 and CaO [9]. On the other hand, we find the acceptorlike Ti vacancies \square_{Ti} to be scarce, because they have high formation energies except under Ti-poor–O-rich conditions when the Fermi level is high in the gap (Fig. 2).

Doping by niobium and tantalum.—The d -orbital projected local DOS of substitutional Nb_{Ti} (Fig. 4) reveals that this single donor does not introduce gap levels like \square_{O} and Ti_i , but that the $4d$ atomic orbitals introduce instead a broad resonance in the conduction band, thereby releasing the excess electron into the TiO_2 conduction band. Thus, Nb_{Ti} fulfills the requirement for shallow, conductive defects according to our previously developed classification scheme [13]. Tantalum, Ta_{Ti} (not shown in Fig. 4), behaves similarly. Indeed, the calculated $(0/+)$ donor levels of Nb_{Ti} and Ta_{Ti} are very shallow, i.e., at $\epsilon(0/+) = E_c - 0.01$ eV (Fig. 2). Because of the low formation energy of Nb_{Ti} and Ta_{Ti} under Ti-rich–O-poor conditions (Fig. 2), the Nb and Ta solubility is high, i.e., 2×10^{21} cm^{-3} and 4×10^{21} cm^{-3} , respectively, as shown in Fig. 5. Because of the high formation energy of the compensating \square_{Ti} acceptor, these n -doping levels remain uncompensated under maximally Ti-rich conditions, i.e., for low $p(\text{O}_2)$.

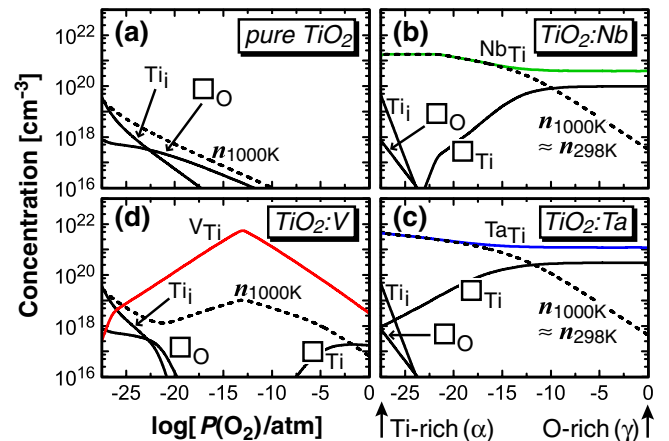


FIG. 5 (color online). Calculated defect and free electron ($n_{1000\text{ K}}$) densities in (a) undoped TiO_2 , and TiO_2 doped by (b) Nb, (c) Ta, and (d) V, shown as a function of the oxygen partial pressure $p(\text{O}_2)$ for $T_{\text{growth}} = 1000$ K. The Ti-rich and O-rich limits (lines “ α ” and “ γ ” in Fig. 3, respectively) are indicated. The room-temperature electron density $n_{298\text{ K}}$ is obtained by “freezing” the respective equilibrium defect densities at 1000 K. Because of deep donor levels, $n_{298\text{ K}} \leq 10^{14}$ cm^{-3} in pure and V-doped TiO_2 (a + d).

Only at intermediate and O-rich conditions $p(\text{O}_2) \geq 10^{-15}$ atm, the electron density falls considerably short of the Nb and Ta dopant density. Thus, TiO_2 shows sufficient resilience against the spontaneous formation of “electron killers” [8] (i.e., intrinsic acceptors) under Ti-rich conditions. These calculations explain the experimental observations of Refs. [5–7] in thin TiO_2 : Nb, Ta films grown by pulsed laser deposition, where the free electron concentration is in the range of 1×10^{19} to 2×10^{21} cm^{-3} for Nb doping and 2.9×10^{20} to 3.2×10^{21} cm^{-3} for Ta doping.

Doping by vanadium.—Figure 4 shows that V_{Ti} introduces deep levels in the gap, which is a consequence of the relatively low $3d$ energy of the V atom (Fig. 1). The corresponding donor level at $\epsilon(0/+) = E_c - 1.36$ eV leads to small room-temperature electron densities (Fig. 5). Thus, V-doped TiO_2 is nonconductive. However, the $t_{2+}^1 t_{2-}^0 e_+^0 e_-^0$ electronic configuration implies a partially occupied, spin-polarized level with a magnetic moment of $1 \mu_B$, which could promote ferromagnetism [15]. Indeed, an experimental study [25] on TiO_2 : V found ferromagnetic behavior. We here find ferromagnetic coupling between two V_{Ti}^0 impurities, with a ferromagnetic stabilization energy of $\Delta E_{\text{FM}} = E_{\text{AFM}} - E_{\text{FM}} = 124, 48, 104, 24, 27$ for the first, second, third, fourth, and fifth neighbors, respectively [24]. Previous LDA + U studies [26,27] indicated a somewhat smaller magnetic stabilization energy, $\Delta E_{\text{FM}} = 34$ meV [26] and 29 meV [27], for the first neighbor, but a systematic study of the range of interaction was not carried out.

The question is now whether magnetic percolation can be achieved by the thermodynamic solubility of vanadium. Figure 5 shows that the maximal V concentration is 6×10^{21} cm^{-3} or 21% of the Ti lattice sites. This maximal V concentration is obtained for $\Delta\mu_{\text{O}} = -2.39$ eV [i.e., $p(\text{O}_2) = 9 \times 10^{-14}$ atm at $T_{\text{growth}} = 1000$ K], corresponding to phase coexistence of the competing V_2O_3 and V_2O_5 phases, as shown in Fig. 3. Since we established before [17] that the minimum concentration $x_{\text{perc}} = 5.6\%$ assures wall-to-wall percolation for fifth-neighbor interaction in the anatase lattice, we expect magnetic percolation and ferromagnetism in TiO_2 : V.

In conclusion, we studied theoretically the two distinct types of electronic behaviors in wide-gap oxides doped with d transition-metal impurities, specifically column V-B transition-metal dopants in anatase TiO_2 : (i) Because of the high atomic d -orbital energy of niobium and tantalum, Nb_{Ti} and Ta_{Ti} release their electrons to the TiO_2 conduction band, and lead to transparent conductivity; (ii) because of the lower d -orbital energy of vanadium, V_{Ti} introduces a spin-polarized gap state, leading to ferromagnetic V-V coupling. We predict uncompensated electron densities above 10^{21} cm^{-3} for Nb and Ta doping, and V solubility above the magnetic percolation threshold.

This work was funded by DARPA under NREL Contract No. DE-AC36-99GO10337.

-
- [1] M. Sacerdoti *et al.*, J. Solid State Chem. **177**, 1781 (2004).
 - [2] F. Gracia, J. Holgado, A. Caballero, and A. Gonzales-Elipe, J. Phys. Chem. B **108**, 17466 (2004).
 - [3] Y. Matsumoto *et al.*, Science **291**, 854 (2001).
 - [4] L.-H. Ye and A. Freeman, Phys. Rev. B **73**, 081304(R) (2006).
 - [5] Y. Furubayashi *et al.*, Appl. Phys. Lett. **86**, 252101 (2005).
 - [6] T. Hitosugi *et al.*, Jpn. J. Appl. Phys. **44**, L1063 (2005).
 - [7] M. Gillispie, M. van Hest, M. Dabney, J. Perkins, and D. Ginley, J. Mater. Res. **22**, 2832 (2007); J. Appl. Phys. **101**, 033125 (2007).
 - [8] A. Zunger, Appl. Phys. Lett. **83**, 57 (2003).
 - [9] J. Osorio-Guillén, S. Lany, S. Barabash, and A. Zunger, Phys. Rev. Lett. **96**, 107203 (2006).
 - [10] L. Forro, O. Chauvet, D. Emin, L. Zuppiroli, H. Berger, and F. Lévy, J. Appl. Phys. **75**, 633 (1994).
 - [11] T. Sekiya *et al.*, J. Phys. Soc. Jpn. **73**, 703 (2004).
 - [12] Ç. Kiliç and A. Zunger, Appl. Phys. Lett. **81**, 73 (2002).
 - [13] S. Lany and A. Zunger, Phys. Rev. B **72**, 035215 (2005).
 - [14] L. Visscher and K. Dyllal, At. Data Nucl. Data Tables **67**, 207 (1997).
 - [15] P. Mahadevan, A. Zunger, and D. Sarma, Phys. Rev. Lett. **93**, 177201 (2004).
 - [16] A. Franceschetti *et al.*, Phys. Rev. Lett. **97**, 047202 (2006).
 - [17] J. Osorio-Guillén, S. Lany, S. Barabash, and A. Zunger, Phys. Rev. B **75**, 184421 (2007).
 - [18] G. Kresse and D. Joubert, Phys. Rev. B **59**, 1758 (1999).
 - [19] C. Persson, Y.-J. Zhao, S. Lany, and A. Zunger, Phys. Rev. B **72**, 035211 (2005).
 - [20] H. Tang, F. Lévy, H. Berger, and P. Schmid, Phys. Rev. B **52**, 7771 (1995).
 - [21] S. Lany and A. Zunger, Phys. Rev. Lett. **98**, 045501 (2007).
 - [22] S. Na-Phattalung *et al.*, Phys. Rev. B **73**, 125205 (2006).
 - [23] V. Anisimov *et al.*, J. Phys. Condens. Matter **18**, 1695 (2006).
 - [24] While the LDA + U or GGA + U methods generally improve the description of the electronic structure for transition metals in insulators, the appropriate value of the Hubbard U is generally not precisely known. Treating U as a free parameter, we find the trend that the band gap increases with U , but the defect levels of \square_{O} and Ti_i do not follow this shift and, hence, become deeper due to this correction. For V_{Ti} , we find that the defect state moves down in the gap, which possibly leads to stronger localization and more short-ranged magnetic interaction.
 - [25] N. Hong, J. Sakai, and A. Hassini, Appl. Phys. Lett. **84**, 2602 (2004).
 - [26] Y. Wang and D. Doren, Solid State Commun. **136**, 142 (2005).
 - [27] X. Du, Q. Li, H. Su, and J. Yang, Phys. Rev. B **74**, 233201 (2006).